HHS Public Access

Author manuscript

Nat Struct Mol Biol. Author manuscript; available in PMC 2015 March 02.

Published in final edited form as:

Nat Struct Mol Biol. 2014 November ; 21(11): 1006–1012. doi:10.1038/nsmb.2894.

A Mechanism for Intracellular Release of Na^+ by Neurotransmitter: Sodium Symporters

Lina Malinauskaite[1,2], **Matthias Quick**[3,4,6], **Linda Reinhard**[1,7], **Joseph A. Lyons**[1,2], **Hideaki Yano**[3,8], **Jonathan A. Javitch**[3,4,5,6], and **Poul Nissen**[1,2]

Matthias Quick: mq2102@columbia.edu; Poul Nissen: pn@mb.au.dk

[1]Danish Research Institute of Translational Neuroscience - DANDRITE, Nordic-EMBL Partnership for Molecular Medicine

[2]Dept. of Molecular Biology and Genetics, Aarhus University, Gustav Wieds Vej 10 C, DK-8000 Aarhus C, Denmark

[3]Center for Molecular Recognition, Columbia University College of Physicians and Surgeons, New York, NY 10032, USA

[4]Department of Psychiatry, Columbia University College of Physicians and Surgeons, New York, NY 10032, USA

[5]Pharmacology, Columbia University College of Physicians and Surgeons, New York, NY 10032, USA

[6]Division of Molecular Therapeutics, New York State Psychiatric Institute, New York, NY, 10032 USA

Abstract

Neurotransmitter:sodium symporters (NSS) terminate synaptic signal transmission by Na^+-dependent reuptake of released neurotransmitters, with key conformational states reported for a bacterial homolog LeuT and an inhibitor-bound *Drosophila* dopamine transporter. However, a coherent mechanism of Na^+-driven transport has not been described. Here, we present two crystal structures of MhsT, a NSS member from *Bacillus halodurans*, in occluded inward-facing states with bound Na^+ ions and L-Trp that provide insight into the cytoplasmic release of Na^+. The switch from outward- to inward-oriented states is centered on the partial unwinding of transmembrane helix 5, which is facilitated by a conserved $GlyX_9Pro$ motif that opens an intracellular pathway for water to access the Na2 site. Based on our structural and functional findings we propose a mechanism according to which solvation through the TM5 pathway facilitates Na^+ release from Na2 and the transition to an inward-open state.

Correspondence to: Matthias Quick, mq2102@columbia.edu; Poul Nissen, pn@mb.au.dk.

[7]Current address: Department of Cell and Molecular Biology, Karolinska Institutet. Box 285, 17177 Stockholm, Sweden and Department of Cell and Molecular Biology, Karolinska Institutet, Notkestrasse 85, 22607 Hamburg, Germany

[8]Current address: National Institute on Drug Abuse, Intramural Research Program, National Institutes of Health, Department of Health and Human Services, Baltimore, MD 21224, USA

Author Contributions: The functional characterization was performed by M.Q., H.Y. and L.M. HiLiDe crystallization, data collection and structure determination was performed by L.M. and assisted by L.R. LCP crystallization and data collection was performed by L.M. and J.A.L. and structure determination by L.M. The manuscript was written by L.M., M.Q., J.A.J, and P.N. and all authors commented on the manuscript.

Introduction

The neurotransmitter: sodium symporter (NSS) family encompasses a large group of prokaryotic and eukaryotic proteins that exploit the energy stored in the Na^+ electrochemical gradient to power the uphill transport of their respective substrates[1-3]. Whereas bacterial NSS mediate the Na^+-coupled uptake of amino acids, many human NSS (also known as the SLC6 family)[4] are expressed in presynaptic neurons where they perform the Na^+/Cl^--coupled reuptake of neurotransmitters such as serotonin, dopamine, γ -aminobutyric acid (GABA) and glycine from the synaptic cleft[2,3]. Notably, SLC6 members are therapeutic drug targets for the treatment of a broad range of neuropsychiatric conditions including depression, epilepsy and ADHD[5,6] as well as being targets for widely abused psychostimulants such as cocaine and amphetamine[6].

Crystal structures of the *Aquifex aeolicus* amino acid transporter LeuT[7-10] have revealed the general structure of NSS showing an inverted pseudo-twofold symmetry relating two transmembrane domains comprising of transmembrane helices (TMs) 1-5 and 6-10, respectively. The Na1 and Na2 binding sites as well as the primary substrate-binding site (S1) are situated between the so-called scaffold (TMs 3-4, 8-9) and bundle domains (TMs 1-2, 6-7)[7]. The available structures for LeuT have revealed a number of the main states proposed to be involved in the transport cycle of the NSS family: outward-open with bound Na^+ (ref. 10), occluded outward-oriented with bound Na^+- and L-Leu[7], and an inward-open apo state[10]. The inhibitor-bound, outward-open *Drosophila melanogaster* dopamine transporter (dDAT) structure[11] is similar to LeuT, indicating that the general mechanism of transport is conserved across the NSS family.

Despite the lack of significant sequence identity, the LeuT-fold architecture[12,13] is shared by several transporter families that extend beyond the NSS family[7,10,14-19]. Notably, the Na2 site of LeuT is conserved as a Na^+ or H^+ binding site in different transporters, highlighting its central role as the essential driver of ion-coupled transport in LeuT-fold transporters in general[7,10,14-17].

However, fundamental questions addressing the transition from the substrate-bound, outward-facing occluded state[7] to the substrate-free, inward-facing[10] state and how it is coupled to the driving Na^+ gradient have in fact remained unanswered for the NSS family and other Na^+-driven transporters. Here we report the first crystal structures of a NSS member in an occluded inward-facing state with bound Na^+ and substrate, namely the *Bacillus halodurans* multi-hydrophobic amino acid transporter (MhsT) determined at 2.1 Å and 2.6 Å resolution using two lipid-based crystallization methods, *i.e.*, using detergent-solubilized lipids (HiLiDe)[20] and lipidic cubic phase (LCP)[21], respectively (Table 1; Fig. 1).

Results

MhsT substrate transport and binding

MhsT, a NSS homolog from *Bacillus halodurans*, is a transporter for hydrophobic L-amino acids[22] (Fig. 2a). Transport of L-Trp in MhsT-containing proteoliposomes is time-dependent

(Fig. 2b) and saturable with a K_t (substrate concentration at half-maximum transport velocity) of 1.7 ± 0.3 μM and a V_{max} (maximum transport velocity) of 0.95 ± 0.04 μmol × mg MhsT^{-1} × min^{-1}, yielding a catalytic turnover number (k_{cat}) of 0.8 ± 0.03 s^{-1} (Fig. 2c). This number is similar to many other Na^+-coupled transporters[22-24] but about two and three orders of magnitude faster than LeuT-mediated transport of L-Ala and L-Leu, respectively[7,25]. MhsT binds L-Trp with an apparent K_d (dissociation constant) value of 4.8 ± 0.6 μM and a molar binding stoichiometry of 1.1 ± 0.04 as determined by saturation equilibrium binding studies in dodecylmaltoside (DDM), the detergent we used for solubilization and purification of MhsT (Fig. 2d).

Two MhsT crystal structures

We obtained two independent crystal forms of MhsT using HiLiDe[20] (Fig. 1a and b; Table 1) and LCP[21] crystallization methods (Fig. 1c; Table 1) with the resulting structures determined at 2.1 and 2.6 Å resolution, respectively. Both structures represent an occluded state with two bound Na^+ ions and one L-Trp molecule (Fig. 1; Table 1). The structures are overall similar and superimpose with a 0.65 Å r.m.s.d., but differ at a specific, local region (see below). In the following MhsT and MhsT^{LCP} will refer to the HiLiDe and the LCP structures, respectively.

Functional state of the MhsT structure

The overall fold of MhsT is similar to LeuT[7] (Supplementary Fig. 1) and dDAT[11], with which it shares 33% and 25% sequence identity, respectively (see Supplementary Discussion). Similar to the inward-open conformation of LeuT[10] we observe a tight hydrophobic cluster of TM1b, 2, 6a and 7 that effectively seals the extracellular side of the transporter (Fig. 3b and c). Thus, compared to the occluded outward-facing state of LeuT[7], which displays an open and hydrophobic extracellular vestibule, the extracellular vestibule of MhsT is collapsed. Interestingly at the intracellular side, we observe a water access pathway that reaches the Na2 site (Fig. 1a), while the bound substrate and Na1 site remain inaccessible. Thus, the MhsT structure represents an occluded, inward-facing state (see below).

The collapsed extracellular vestibule forms a hydrophobic cluster centered on Trp33 of TM1b (Fig. 3b and c), which is conserved across the NSS family except for LeuT that has Leu29^{LeuT} at the equivalent position (Supplementary Fig. 2a). The bulky nature of Trp33 leaves no void for an additional ligand, in contrast to the inward-open state of LeuT, which also displays extracellular closure, but with a yet unidentified entity enclosed near Leu29^{LeuT} (ref. 10) and possibly marks a second substrate site (S2) as previously identified by molecular dynamics simulations and functional studies[25].

A number of structures of non-NSS LeuT-fold transporters have also been assigned as occluded and inward-facing, including a Na^+ -released, galactose-bound vSGLT[14,26,27], a Na^+ -released betaine-displaced BetP[17,28] and a post-substrate released ApcT in a return state[16]. All of these models therefore represent later intermediates of a transport cycle than the Na^+-bound and occluded inward-facing states reported here for the NSS family transporter MhsT.

Substrate and Na1 binding sites

The binding site for L-Trp in MhsT is similar to the L-Leu occupied S1 site in LeuT[7] (Supplementary Fig. 3a and b). The carboxyl and amino groups of L-Trp make hydrogen bonds with the side chains of Tyr108 and Ser233 and backbone atoms of Gly30, Ala26, Thr231 and Phe230. A flexible Met236 side chain accommodates the bulky indole group of L-Trp, and the indole nitrogen makes a hydrogen bond with Ser327 (Supplementary Fig. 3a). Comparing MhsT and LeuT, the bulky side chains of $Phe259^{LeuT}$ and $Ile359^{LeuT}$ ($Met236^{MhsT}$ and $Leu328^{MhsT}$, respectively) cannot accommodate L-Trp[8] (Supplementary Fig. 3d), and although a $Ile359Gln^{LeuT}$ mutation supports L-Trp transport and binding[29] it imposes a different rotamer configuration of L-Trp (Supplementary Fig. 3c) than in the L-Trp-transporting MhsT (Supplementary Fig. 3a). The coordination of Na1 in MhsT is similar to LeuT[7] (Supplementary Table 1), showing octahedral geometry by side chains of Asn31, Thr231 and Asp263, backbone carbonyls of Ala26 and Thr231, as well as the L-Trp carboxyl group (Supplementary Fig. 3e and f).

TM5 unwinding and intracellular access to the Na2 site

Unlike the inward-open conformation of LeuT[10], the extracellular closure of MhsT is not paired with an open configuration of the intracellular side (Fig. 3b and c; Fig. 4a). Rather, the intracellular side is reminiscent of the outward-facing states[7,10] (Fig. 3a; Fig. 4a and c), where the N-terminal tail seals the cytoplasmic side through specific, polar interactions and with Trp12 ($Trp8^{LeuT}$, conserved across the NSS family) plugging a hydrophobic pocket (Fig. 4a and b; Supplementary Fig. 4). However, the intracellular side also differs in key details from that of the outward-facing forms of LeuT. Most importantly, we observe unwinding of the intracellular part of TM5 – a feature that creates a solvent pathway that provides water access from the cytoplasm to the Na2 site (Fig. 4a; Supplementary Fig. 4b and see below). We propose that the unwinding results from the strain imposed by the movement of the extracellular part of TM5 (TM5e) together with TM6a in closure of the extracellular vestibule around Trp33, while at the same time the intracellular part of TM5 (TM5i) holds on to a short coiled-coil interaction with TM1a, which in turn is held in place through coordination with Na^+ at the Na2 site (Fig. 4a-c). Furthermore, the negative end of TM4 and the positive end of TM5i dipoles[30] interact with the salt bridge between the conserved $Arg344^{MhsT}$ ($Arg375^{LeuT}$) of the TM8-9 loop and $Glu10^{MhsT}$ ($Glu6^{LeuT}$) of the N-terminal end, respectively (Fig. 4a and c; Supplementary Fig. 4). Thus, the substrate-occluding configuration of the intracellular interface is dependent on the occupied Na2 site, which promotes the TM1a enclosure of the Na1 and L-Trp binding sites (Fig. 4a, see below).

Importantly, the unwinding of TM5 is likely facilitated by a conserved $GlyX_9Pro$ helix-breaking motif ($Gly171X_9Pro181^{MhsT}$, $Gly190X_9Pro200^{LeuT}$, Fig. 5a). A sequence alignment of NSS for the poorly conserved TM4-TM5 region[31] was confirmed and further refined by the recent dDAT structure[11]. This alignment indicates two populations for the $GlyX_9Pro$ motif, where in mammalian NSS it is slightly shifted in position with respect to bacterial NSS (Fig. 5a; Supplementary Fig. 2). However, we predict a preserved ability to promote unravelling of TM5i as observed here. We speculate that the sequence variations

fine-tune the TM5 deformation mechanism to the specific physico-chemical conditions of individual species.

Interestingly, structural alignment of MhsT (NSS family) and Mhp1[15] (nucleobase:cation symporter-1 (NCS1) family), which is another LeuT-fold transporter, reveals a recurring $GlyX_nPro$ pattern in the intracellular part of TM5 (Supplementary Fig. 5), suggesting that the unwinding and cytoplasmic water access to the Na^+ binding site in the inward-facing states may also be exploited in other Na^+-dependent, LeuT-fold transporters (See Supplementary Discussion for additional details on structural alignment of other LeuT-fold symporters).

Na2 solvation

In the occluded outward-facing state of LeuT the Na^+ ion at the Na2 site is buried and has trigonal-bipyramidal coordination by five ligands[7]. However, for MhsT a cytoplasmic water molecule is added as a sixth ligand, which accesses Na2 through the solvent pathway afforded by TM5 unwinding (Fig. 1 and 4; Supplementary Table 1). TM8 is displaced with respect to TM1, and the Ser323 side chain has shifted, providing space for the water molecule. The equivalent $Thr354^{LeuT}$ has previously been suggested to be important for Na2 solvation[32]. With this additional water ligand, Na2 has changed coordination chemistry from trigonal-bipyramidal and occluded to octahedral yet distorted (Fig. 4b), and is now in contact with the intracellular environment. The Na2 site is, therefore, effectively primed for further solvation and Na^+ release to the cytoplasmic milieu; a process that may be facilitated by the negative membrane potential.

MhsT Trp33 and $GlyX_9Pro$ mutational study

Functionally important residues in MhsT were tested by mutagenesis and measurement of L-Trp uptake into intact *E. coli* (MQ614 strain) cells. The mutation of $Trp33^{MhsT}$ to Leu reduced the V_{max} by nearly 70% compared to MhsT-WT with little effect on K_t (Fig. 5b and c). These findings support a role for the conserved Trp33 in enhancing the transition to the inward-facing conformation. Notably, for the mammalian γ-aminobutyric acid (GABA) transporter GAT1 the corresponding $Trp68Leu^{GAT1}$ mutation shows unaffected ligand binding affinity yet markedly reduced transport due to impaired substrate release[33]. In addition, mutation of the aligned residue in human DAT ($Trp85Leu/Ala^{hDAT}$) enhanced cocaine binding, consistent with a more outward-open configuration, and reduced transport by slowing inward release of dopamine[34,35].

Similarly, the functional role of the $Gly171X_9Pro181$ motif in MhsT was investigated. Mutating Gly171 to Ala or Pro181 to Leu drastically reduced the uptake of ^{3}H-Trp (Fig. 5b and c) with V_{max} values that were 97.2±0.2% and 93.2±1.8% lower than the V_{max} for WT, respectively, while the K_t was 3.8 times higher for Gly171Ala and 2.4 times lower for the Pro181Leu mutant compared to WT (Fig. 5c). $Pro272^{rDAT}$ of the TM5-$GlyX_9Pro$ motif of the rat dopamine transporter was previously shown to be important for the apparent affinity for dopamine and a cocaine analog, and for the turnover of dopamine transport[36], all consistent with a central role for this structural motif in transport. Also of note, hSERT is

activated by protein kinase G phosphorylation of Thr276, which precedes the $Gly278X_9Pro288^{hSERT}$ motif[37] hinting at a regulatory interplay.

Thus, mutations of the $GlyX_9Pro$ motif primarily reduce the V_{max}, and have smaller and diverse effects on the K_t, suggesting that such mutant forms generally allow binding of substrate in the outward open state but are impaired in the forward transition towards substrate release.

Differences between MhsT and $MhsT^{LCP}$ structures

Comparing our two independent crystal forms of the occluded, inward-facing state we note that the $MhsT^{LCP}$ structure exhibits tighter crystal packing (Supplementary Fig. 6) and a displaced N-terminal segment that is disordered in the crystal structure (Fig. 1b and c). Without the N-terminal segment stabilizing the unwound TM5 the latter reverts to a continuous but slightly kinked helix (Fig. 1c; Supplementary Fig. 6e; Supplementary Movie 1), similar to that observed in the LeuT[7,10] and dDAT[11] structures. The helical TM5 now disconnects the solvent pathway from the cytoplasm to the Na2 site. Importantly, the $MhsT^{LCP}$ structure therefore shows that TM5 of MhsT is capable of forming a helix as observed in LeuT and dDAT while also highlighting that conserved features of the N-terminal segment are important for stabilization of a conformation that opens the Na2 site to the cytoplasm (Supplementary Movie 1). Dynamics of the N-terminal segment have also been observed in single-molecule studies as being integral to function[38]. Furthermore we note that the continuous TM5 helix thus formed upon N-terminal tail disengagement remains flexible as indicated by high displacement factors for that region in the $MhsT^{LCP}$ structure (Fig. 1c).

Comparison of the MhsT, $MhsT^{LCP}$ and LeuT structures[7,10] therefore suggests a “spring mechanism” for Na^+ release (Fig. 4a): the TM5 helix is continuous in the occluded outward-facing state[7], then exploits unwound conformations as an extended spring (or other flexible conformations) in the inward-facing state observed here, and finally reforms as a continuous helix in the inward-open state upon Na^+ and substrate release[10].

Discussion

The MhsT structures reported here provide new insights into the coupling of Na^+ and substrate release for the NSS family. A coupled mechanism has been proposed for secondary transporters where the driving ion binds before the main substrate (‘first-on’) in the outward-facing state and has to be released before the main substrate (‘first-off’) in the inward-oriented state[13,39]. Functional studies of the NSS family have shown that Na^+ binding stabilizes the outward-open state and precedes substrate binding[38,40-42]. This model was confirmed by the crystal structure of the Na^+-bound outward-open state of LeuT[10]. Furthermore, molecular dynamics simulations of LeuT for the occluded, outward-facing state proposed that cytoplasmic water access to the Na2 site primes substrate release[32]. The MhsT structures presented here provides experimental support for this, but through an unanticipated mechanism, namely TM5 unwinding.

A related release mechanism was recently proposed for a Major Facilitator Superfamily transporter, namely the proton-dependent phosphate transporter PiPT[43]. For PiPT an occluded inward-facing state displays a narrow putative H^+ release pathway, suggesting also a two-step intracellular release mechanism: firstly of the driving H^+ through the narrow pathway formed upon substrate occlusion, and secondly of the transported substrate as H^+ release triggers inward opening.

In conclusion, our observations suggest a general model of NSS function (Fig. 6; Supplementary Movie 2): First, Na^+ and substrate binding in an outward-open state initiates occlusion by interactions with TM1b and TM6a[7]. This occluded, outward-facing state exposes a hydrophobic vestibule, which primes the transporter for further, extracellular closure upon movement of TM1b, TM6a TM7 and EL4 together with TM5e that at the same time drives the transporter towards the inward-facing state presented here. The extracellular closure is centered on the conserved $Trp33^{MhsT}$ of TM1, but may involve binding of a second substrate (S2) in LeuT[9,10], which lacks the conserved Trp at this position. In the occluded inward-facing state, TM5e has moved relative to TM5i, which maintains its interaction with the N-terminal segment and TM1a through joint coordination of Na^+ at the Na2 site (Fig. 4b); TM5 therefore extends as a spring at the cytoplasmic membrane interface, with the unwinding facilitated by the conserved $GlyX_9Pro$ deformation points. TM5 unwinding however provides access of intracellular solvent to the Na2 site, with the Na2 site accepting a water molecule as a sixth ligand, completing octahedral coordination (Fig. 4b; Supplementary Fig. 3g and h). The occluded inward-facing state is therefore primed for full solvation and intracellular release of Na^+ from the Na2 site. Due to the low intracellular concentration of Na^+, maintained by active Na^+ extruding transporters, the intracellular release of Na2 triggers the forward reaction. Once Na2 is released, possibly stimulated by the structural flexibility of TM5 and a negative membrane potential, TM1a becomes liberated and can swing out while TM5i reassociates with TM5e in reformation of the TM5 helix, which in combination provides the opening for substrate and Na1 release to the intracellular environment[10].

Thus the MhsT structures provide a missing link that depicts in concrete structural terms how an intimate sequence of intermediate steps during the transport cycle of a secondary transporter is connected to the downhill movement of Na^+ along its transmembrane electrochemical gradient. Furthermore, these structures suggest that the dynamics of such individual states play another key role, with further studies of structure, function and dynamics required to establish a comprehensive understanding of how membrane transporter molecules work in a biomembrane.

Methods

Protein expression and purification

The *mhsT* gene flanked by a sequence that encodes an N-terminal 10×His tag and TEV protease cleavage site (in plasmid pNZ8048) was expressed in *Lactococcus lactis* NZ9000 and purified as previously described[22].

Transport in proteoliposomes and intact cells

Transport of ^{3}H-Trp in intact *E. coli* MQ614 [*aroP mtr tnaB tyrP1 pheP::cat*] was performed as described[44]. For uptake studies in proteoliposomes purified MhsT was reconstituted at a 1:150 (w/w) ratio in preformed liposomes made from *E. coli* polar lipid extract (Avanti Polar Lipids) that were destabilized with 1.7 mM Triton X-100[22,24]. Detergent was removed by stepwise addition of a total of 240 mg/mL Bio-Beads SM-2 (Biorad) and the proteoliposomes (or control liposomes) were collected by ultracentifugation at 320,000 × *g* for 45 min, resuspended (to ∼100 mg lipids/mL) in 100 mM potassium phosphate pH 6.5, 1 mM TCEP and stored in liquid N_2. Prior to uptake measurements the proteoliposomes were thawed at 23 °C and extruded through a 400 nm filter (Avanti). The accumulation of ^{3}H-Trp (20 Ci/mmol; American Radiolabeled Chemicals, Inc.) was measured with increasing concentrations of ^{3}H-Trp (2 Ci/mmol) for the indicated periods of time at 22 °C in assay buffer composed of 10 mM Tris/MES pH 8.5, 50 mM NaCl in the presence of 1 μM valinomycin. To determine ^{3}H-Trp binding to the MhsT-containing proteoliposomes or to control liposomes, the time course of ^{3}H-Trp uptake was performed by dissipating the electrochemical NaCl gradient with gramicidin (25 μg/mL) for 5 min prior to the start of the reaction. Reactions were stopped by ice-cold assay buffer followed by rapid filtration through 0.22 μm nitrocellulose filters (Millipore) and used for scintillation counting. Counts per minute (cpm) were transformed into pmol using known amounts of ^{3}H-Trp. Protein incorporated in proteoliposomes (as well as in detergent-solubilized form) was assayed using the amidoblack protein assay[45].

Binding studies

Saturation binding of ^{3}H-Trp to MhsT purified in *n*-dodecyl-β,D-maltopyranoside (DDM, Anagrade, Anatrace) was performed as described[22] by means of the scintillation proximity assay (SPA) with 4.1 pmol of purified protein per assay in buffer composed of 150 mM Tris/MES pH 7.5, 50 mM NaCl, 1 mM TCEP, 20% glycerol, and 2 mM DDM. Samples were incubated with increasing concentrations of radioligand and measured in the SPA cpm mode of the MicroBeta™ counter. The efficiency of detection was calculated with a standard curve of known concentration to transform cpm into pmol. Specific binding was determined by subtracting the non-proximity signal (as determined in the presence of 800 mM imidazole) from the total binding, and was plotted as a function of free radioligand. Nonlinear regression fitting of the data was performed to obtain the K_d (concentration at 50% maximum binding) and molar ratio of Trp-to-MhsT binding (Graphpad Prism5).

Crystallization, data collection and processing

For crystallization experiments MhsT purified in DDM (SOL-GRADE, Anatrace) was digested with TEV protease to remove the His-tag and loaded on a second Ni-column (Ni-NTA, Qiagen) collecting the MhsT-containing flow-through. The protein was concentrated using a Viva-spin concentration device with molecular weight (MW) cut-off of 50 kDa to 7 mg/mL for size exclusion chromatography on a TSKgel G3000SW (Tosoh Bioscience) column with a running buffer consisting of 10 mM Tris-HCl pH 7.0, 100 mM NaCl, 10% (v/v) glycerol, 0.5 mM L-tryptophan (Sigma), 0.35 mM DDM. Peak fractions were collected and concentrated to 9-10 mg/mL using a Viva-spin concentration device with a MW cut-off

of 50 kDa. MhsT was re-lipidated by adding 1,2-dioleoyl-sn-glycero-3-phosphocholine (DOPC, Sigma) lipids according to the HiLiDe method[20] with a 6:1 protein to lipids weight ratio.

A reservoir buffer containing 100 mM Tris-HCl pH 7.0, 400 mM NaCl, 20-24% w/w PEG400 and 5% trimethylamine-N-oxide (Sigma), supplemented with 11 mM *n*-nonyl-β-D-glucoside (NG, Anagrade, Anatrace) was mixed with the protein solution as 1 + 1 μL drops and subjected to vapor diffusion at 19 °C in hanging drops sealed with immersion oil[20]. Mounted crystals were subjected to controlled dehydration[46] with a HC1c humidity control device at BESSY II beamline BL14.3[47], reducing humidity from 93% to 89% in 1% steps with 2 min incubation prior to flash cooling in liquid N_2. X-ray diffraction data were collected at 0.8726 Å wavelength at the ESRF ID23-2 microfocus beamline and processed in space group P2 using the XDS package[48] and TRUNCATE[49] yielding a final dataset at 2.1 Å resolution as judged from the Wilson plot (with Wilson B-factor 27.8), the $CC_{1/2}$ coefficient and model refinement statistics (see Table 1).

The MhsT reconstituted lipidic cubic phase (LCP) was prepared by the two syringe method[21,50] by mixing 7.8 MAG (1-(7Z-pentadecenoyl)-rac-glycerol, Avanti Polar Lipids) lipid with protein (10 mg/mL) in a 1:1 weight ratio of protein solution to lipid. Crystallization trials were set up using an LCP dispensing robot (LCP Gryphon, Art Robbins Instruments) with the LCP dispensed on to homemade silanized 96-well glass sandwich crystallization plates with well diameter of 6 mm and well depth of 140 μm[21]. Each well comprised of 50 nL of LCP with 800 nL crystallization solution. Crystals of the MhsT-Trp complex (30 μm plates) were obtained at 19 °C in a crystallization solution containing 20% PEG400, 400 mM NaCl, 100 mM HEPES pH 7.0. Crystals were harvested directly from the LCP and flash cooled in liquid N_2. X-ray diffraction data was collected at 0.9686 Å wavelength at I24 microfocus beamline (Diamond Light Source) and processed in the C2 space group using the XDS package[48] and TRUNCATE[49] yielding a final data set at 2.6 Å resolution as judged from the Wilson plot (with Wilson B-factor 27.5 $Å^2$), the $CC_{1/2}$ coefficient and model refinement statistics. The quality of the datasets was checked with PHENIX XTRIAGE[51] (see Table 1).

Structure determination and analysis

For MhsT, initial phases were obtained by molecular replacement using the PHENIX MR_ROSETTA[51] program. A search model was prepared with PHENIX SCULPTOR[52] combining the MhsT sequence to the LeuT structure of the occluded outward-facing state (PDB 2A65)[7] using a sequence alignment of MhsT and LeuT prepared with Clustal Omega[53]. The model obtained from PHENIX AUTOBUILD[51] yielded R/R_{free} of 0.31/0.43 using a 2.8 Å resolution preliminary data set of the HiLiDe crystal form. The model was rebuilt manually in COOT[54] using density modification and prime-and-switch maps[55], and refinement of coordinates and individual B-factors using PHENIX REFINE[51]. The intermediate model was reintroduced to PHENIX MR_ROSETTA[51] using the 2.1 Å resolution data set (R/R_{free} 0.31/0.36) followed by manual rebuilding, which led to a final model with R_{work}/R_{free} of 0.191/0.235 and Ramachandran plot favored/outliers 97.5/0.0%. Although waters have been modeled at the Na2 solvent access pathway, there were also

indications of continuous density that could be interpreted as PEG400 or glycerol molecules, both of which were present in the crystallization buffer. However, each of these assignments led to unfavorable clashes with the protein structure. It was concluded that the electron density maps reveal water, PEG400 and glycerol in the solvent pathway at overlapping, partial sites, but that water molecules represent an adequate, single model at the available resolution. Initial phases for the LCP model were obtained by MR using the final HiLiDe model. Iterative rounds of structure refinement were performed in PHENIX REFINE[51] with the models revised in real space with the program COOT[54] leading to R_{work}/R_{free} of 0.201/0.255 and Ramachandran plot favored/outliers 96.5/0.2%. The final refinement statistics are summarized for MhsT HiLiDe and LCP structures in Table 1 (PDB code 4US3 and 4US4, respectively).

Figures were created using PYMOL[56]. The movie was generated from a morph between structures as created using PYMOL[56] with geometry minimization for each iteration performed using PHENIX[51].

A multiple sequence alignment of the NSS family was created using Muscle[57] taking 200 randomly selected scores from a BLAST search on the human serotonin transporter. Using a Blosum30 scoring matrix and a gap open penalty of -45, the sequence alignment reproduced the structural alignment of MhsT, LeuT[7,10] and dDAT[11], in particular for regions showing low sequence identity. This alignment was used for the TM5 analysis of the $GlyX_9Pro$ motif and is essentially identical to a previously published alignment[31]. The structural alignments were performed with DaliLite[58], converted to sequence alignment with Chimera[59] and visualized with Jalview[60]. Electrostatic surface representations were prepared with the Adaptive Poisson-Boltzmann Solver[61].

Supplementary Material

Refer to Web version on PubMed Central for supplementary material.

Acknowledgments

We thank A. M. Winther for her initial work on crystallization of detergent-solubilized MhsT, A.M. Nielsen for technical assistance and J.L. Karlsen for support with scientific computing. We are grateful to L. Shi and H. Weinstein for valuable discussion. We thank S.G. Rasmussen for access to a LCP dispensing robot. We are thankful to D. Flot and S. Russi at the European Synchrotron Radiation Facility ID23-2, and U. Müller and M.S. Weiss at the Helmholtz-Zentrum Berlin synchrotron radiation source BESSY II BL 14.1 and 14.3, and R. Owen and D. Axford at the Diamond Light Source 124, for help with X-ray diffraction data collection. Access to synchrotron facilities were supported by the Danscatt program of the Danish Council for Independent Research and the EU-FP7 infrastructure program Biostruct-X (grants 860 and 5624). This work was supported by research grants of the Lundbeck Foundation and NIH grants DA17293 and DA022413. L.M. was supported by a Boehringer-Ingelheim Fonds fellowship. L.R. was supported by the Danish Council for Independent Research in Medical Sciences and J. A.L. by the Danish Council for Independent Research in Natural Sciences.

References

1. Kristensen AS, et al. SLC6 neurotransmitter transporters: structure, function, and regulation. Pharmacol Rev. 2011; 63:585–640. [PubMed: 21752877]
2. Rudnick, G. Contemporary Neuroscience: Neurotransmitter Transporters: Structure, Function, and Regulation. 2nd. Humana Press Inc.; Totowa, NJ: 2002. Mechanisms of Biogenic Amine Neurotransmitter Transporters; p. 25-51.

3. Torres GE, Gainetdinov RR, Caron MG. Plasma membrane monoamine transporters: structure, regulation and function. Nat Rev Neurosci. 2003; 4:13–25. [PubMed: 12511858]
4. Hediger MA, et al. The ABCs of solute carriers: physiological, pathological and therapeutic implications of human membrane transport proteins Introduction. Pflugers Arch. 2004; 447:465–8. [PubMed: 14624363]
5. Singh SK. LeuT: a prokaryotic stepping stone on the way to a eukaryotic neurotransmitter transporter structure. Channels (Austin). 2008; 2:380–9. [PubMed: 19066470]
6. Gether U, Andersen PH, Larsson OM, Schousboe A. Neurotransmitter transporters: molecular function of important drug targets. Trends Pharmacol Sci. 2006; 27:375–83. [PubMed: 16762425]
7. Yamashita A, Singh SK, Kawate T, Jin Y, Gouaux E. Crystal structure of a bacterial homologue of Na+/Cl--dependent neurotransmitter transporters. Nature. 2005; 437:215–23. [PubMed: 16041361]
8. Singh SK, Piscitelli CL, Yamashita A, Gouaux E. A competitive inhibitor traps LeuT in an open-to-out conformation. Science. 2008; 322:1655–61. [PubMed: 19074341]
9. Quick M, et al. Binding of an octylglucoside detergent molecule in the second substrate (S2) site of LeuT establishes an inhibitor-bound conformation. Proc Natl Acad Sci USA. 2009; 106:5563–8. [PubMed: 19307590]
10. Krishnamurthy H, Gouaux E. X-ray structures of LeuT in substrate-free outward-open and apo inward-open states. Nature. 2012; 481:469–74. [PubMed: 22230955]
11. Penmatsa A, Wang KH, Gouaux E. X-ray structure of dopamine transporter elucidates antidepressant mechanism. Nature. 2013
12. Abramson J, Wright EM. Structure and function of Na(+)-symporters with inverted repeats. Curr Opin Struct Biol. 2009; 19:425–32. [PubMed: 19631523]
13. Forrest LR, Kramer R, Ziegler C. The structural basis of secondary active transport mechanisms. Biochim Biophys Acta. 2011; 1807:167–88. [PubMed: 21029721]
14. Faham S, et al. The crystal structure of a sodium galactose transporter reveals mechanistic insights into Na+/sugar symport. Science. 2008; 321:810–4. [PubMed: 18599740]
15. Weyand S, et al. Structure and molecular mechanism of a nucleobase-cation-symport-1 family transporter. Science. 2008; 322:709–13. [PubMed: 18927357]
16. Shaffer PL, Goehring A, Shankaranarayanan A, Gouaux E. Structure and mechanism of a Na+-independent amino acid transporter. Science. 2009; 325:1010–4. [PubMed: 19608859]
17. Perez C, Koshy C, Yildiz O, Ziegler C. Alternating-access mechanism in conformationally asymmetric trimers of the betaine transporter BetP. Nature. 2012; 490:126–30. [PubMed: 22940865]
18. Tang L, Bai L, Wang WH, Jiang T. Crystal structure of the carnitine transporter and insights into the antiport mechanism. Nat Struct Mol Biol. 2010; 17:492–6. [PubMed: 20357772]
19. Fang Y, et al. Structure of a prokaryotic virtual proton pump at 3.2 A resolution. Nature. 2009; 460:1040–3. [PubMed: 19578361]
20. Gourdon P, et al. HiLiDe—Systematic Approach to Membrane Protein Crystallization in Lipid and Detergent. Crystal Growth & Design. 2011; 11:2098–2106.
21. Caffrey M, Cherezov V. Crystallizing membrane proteins using lipidic mesophases. Nat Protoc. 2009; 4:706–31. [PubMed: 19390528]
22. Quick M, Javitch JA. Monitoring the function of membrane transport proteins in detergent-solubilized form. Proc Natl Acad Sci USA. 2007; 104:3603–8. [PubMed: 17360689]
23. Quick M, Wright EM. Employing Escherichia coli to functionally express, purify, and characterize a human transporter. Proc Natl Acad Sci USA. 2002; 99:8597–601. [PubMed: 12077304]
24. Jung H, Tebbe S, Schmid R, Jung K. Unidirectional reconstitution and characterization of purified Na+/proline transporter of Escherichia coli. Biochemistry. 1998; 37:11083–8. [PubMed: 9693004]
25. Shi L, Quick M, Zhao Y, Weinstein H, Javitch JA. The mechanism of a neurotransmitter:sodium symporter—inward release of Na+ and substrate is triggered by substrate in a second binding site. Mol Cell. 2008; 30:667–77. [PubMed: 18570870]
26. Li J, Tajkhorshid E. Ion-releasing state of a secondary membrane transporter. Biophys J. 2009; 97:L29–31. [PubMed: 19948113]

27. Watanabe A, et al. The mechanism of sodium and substrate release from the binding pocket of vSGLT. Nature. 2010; 468:988–91. [PubMed: 21131949]
28. Ressl S, Terwisscha van Scheltinga AC, Vonrhein C, Ott V, Ziegler C. Molecular basis of transport and regulation in the Na(+)/betaine symporter BetP. Nature. 2009; 458:47–52. [PubMed: 19262666]
29. Piscitelli CL, Gouaux E. Insights into transport mechanism from LeuT engineered to transport tryptophan. EMBO J. 2012; 31:228–35. [PubMed: 21952050]
30. Sengupta D, Behera RN, Smith JC, Ullmann GM. The alpha helix dipole: screened out? Structure. 2005; 13:849–55. [PubMed: 15939016]
31. Beuming T, Shi L, Javitch JA, Weinstein H. A comprehensive structure-based alignment of prokaryotic and eukaryotic neurotransmitter/Na+ symporters (NSS) aids in the use of the LeuT structure to probe NSS structure and function. Mol Pharmacol. 2006; 70:1630–42. [PubMed: 16880288]
32. Zhao C, Noskov SY. The role of local hydration and hydrogen-bonding dynamics in ion and solute release from ion-coupled secondary transporters. Biochemistry. 2011; 50:1848–56. [PubMed: 21265577]
33. Mager S, et al. Ion binding and permeation at the GABA transporter GAT1. J Neurosci. 1996; 16:5405–14. [PubMed: 8757253]
34. Lin Z, Wang W, Uhl GR. Dopamine transporter tryptophan mutants highlight candidate dopamine- and cocaine-selective domains. Mol Pharmacol. 2000; 58:1581–92. [PubMed: 11093799]
35. Chen N, Zhen J, Reith ME. Mutation of Trp84 and Asp313 of the dopamine transporter reveals similar mode of binding interaction for GBR12909 and benztropine as opposed to cocaine. J Neurochem. 2004; 89:853–64. [PubMed: 15140185]
36. Lin Z, Itokawa M, Uhl GR. Dopamine transporter proline mutations influence dopamine uptake, cocaine analog recognition, and expression. FASEB J. 2000; 14:715–28. [PubMed: 10744628]
37. Ramamoorthy S, Samuvel DJ, Buck ER, Rudnick G, Jayanthi LD. Phosphorylation of threonine residue 276 is required for acute regulation of serotonin transporter by cyclic GMP. J Biol Chem. 2007; 282:11639–47. [PubMed: 17310063]
38. Zhao Y, et al. Substrate-modulated gating dynamics in a Na+-coupled neurotransmitter transporter homologue. Nature. 2011; 474:109–13. [PubMed: 21516104]
39. Krupka RM. Coupling mechanisms in active transport. Biochim Biophys Acta. 1993; 1183:105–13. [PubMed: 8399371]
40. Claxton DP, et al. Ion/substrate-dependent conformational dynamics of a bacterial homolog of neurotransmitter: sodium symporters. Nat Struct Mol Biol. 2010; 17:822–9. [PubMed: 20562855]
41. Zhao Y, et al. Single-molecule dynamics of gating in a neurotransmitter transporter homologue. Nature. 2010; 465:188–93. [PubMed: 20463731]
42. Kazmier K, et al. Conformational dynamics of ligand-dependent alternating access in LeuT. Nat Struct Mol Biol. 2014; 21:472–9. [PubMed: 24747939]
43. Pedersen BP, et al. Crystal structure of a eukaryotic phosphate transporter. Nature. 2013; 496:533–6. [PubMed: 23542591]
44. Quick M, et al. State-dependent conformations of the translocation pathway in the tyrosine transporter Tyt1, a novel neurotransmitter: sodium symporter from Fusobacterium nucleatum. J Biol Chem. 2006; 281:26444–54. [PubMed: 16798738]
45. Schaffner W, Weissmann C. A rapid, sensitive, and specific method for the determination of protein in dilute solution. Anal Biochem. 1973; 56:502–14. [PubMed: 4128882]
46. Russi S, et al. Inducing phase changes in crystals of macromolecules: status and perspectives for controlled crystal dehydration. J Struct Biol. 2011; 175:236–43. [PubMed: 21385612]
47. Mueller U, et al. Facilities for macromolecular crystallography at the Helmholtz-Zentrum Berlin. J Synchrotron Radiat. 2012; 19:442–9. [PubMed: 22514183]
48. Kabsch W. Xds. Acta Crystallogr D Biol Crystallogr. 2010; 66:125–32. [PubMed: 20124692]
49. Collaborative Computational Project, N. The CCP4 suite: programs for protein crystallography. Acta Crystallogr D Biol Crystallogr. 1994; 50:760–3. [PubMed: 15299374]

50. Cheng A, Hummel B, Qiu H, Caffrey M. A simple mechanical mixer for small viscous lipid-containing samples. Chem Phys Lipids. 1998; 95:11–21. [PubMed: 9807807]
51. Adams PD, et al. PHENIX: a comprehensive Python-based system for macromolecular structure solution. Acta Crystallogr D Biol Crystallogr. 2010; 66:213–21. [PubMed: 20124702]
52. Bunkoczi G, Read RJ. Improvement of molecular-replacement models with Sculptor. Acta Crystallogr D Biol Crystallogr. 2011; 67:303–12. [PubMed: 21460448]
53. Sievers F, et al. Fast, scalable generation of high-quality protein multiple sequence alignments using Clustal Omega. Mol Syst Biol. 2011; 7:539. [PubMed: 21988835]
54. Emsley P, Lohkamp B, Scott WG, Cowtan K. Features and development of Coot. Acta Crystallogr D Biol Crystallogr. 2010; 66:486–501. [PubMed: 20383002]
55. Terwilliger TC. Using prime-and-switch phasing to reduce model bias in molecular replacement. Acta Crystallogr D Biol Crystallogr. 2004; 60:2144–9. [PubMed: 15572767]
56. Schrodinger LLC. The PyMOL Molecular Graphics System, Version 1.3r1. 2010
57. Edgar RC. MUSCLE: multiple sequence alignment with high accuracy and high throughput. Nucleic Acids Res. 2004; 32:1792–7. [PubMed: 15034147]
58. Holm L, Park J. DaliLite workbench for protein structure comparison. Bioinformatics. 2000; 16:566–7. [PubMed: 10980157]
59. Pettersen EF, et al. UCSF Chimera—a visualization system for exploratory research and analysis. J Comput Chem. 2004; 25:1605–12. [PubMed: 15264254]
60. Waterhouse AM, Procter JB, Martin DM, Clamp M, Barton GJ. Jalview Version 2--a multiple sequence alignment editor and analysis workbench. Bioinformatics. 2009; 25:1189–91. [PubMed: 19151095]
61. Baker NA, Sept D, Joseph S, Holst MJ, McCammon JA. Electrostatics of nanosystems: application to microtubules and the ribosome. Proc Natl Acad Sci USA. 2001; 98:10037–41. [PubMed: 11517324]
62. Forrest LR, Rudnick G. The rocking bundle: a mechanism for ion-coupled solute flux by symmetrical transporters. Physiology (Bethesda). 2009; 24:377–86. [PubMed: 19996368]
63. Zhao Y, et al. Substrate-dependent proton antiport in neurotransmitter:sodium symporters. Nat Chem Biol. 2010; 6:109–16. [PubMed: 20081826]
64. Wohlers I, Andonov R, Klau GW. DALIX: optimal DALI protein structure alignment. IEEE/ACM Trans Comput BiolBioinform. 2013; 10:26–36.
65. Hasegawa H, Holm L. Advances and pitfalls of protein structural alignment. Curr Opin Struct Biol. 2009; 19:341–8. [PubMed: 19481444]

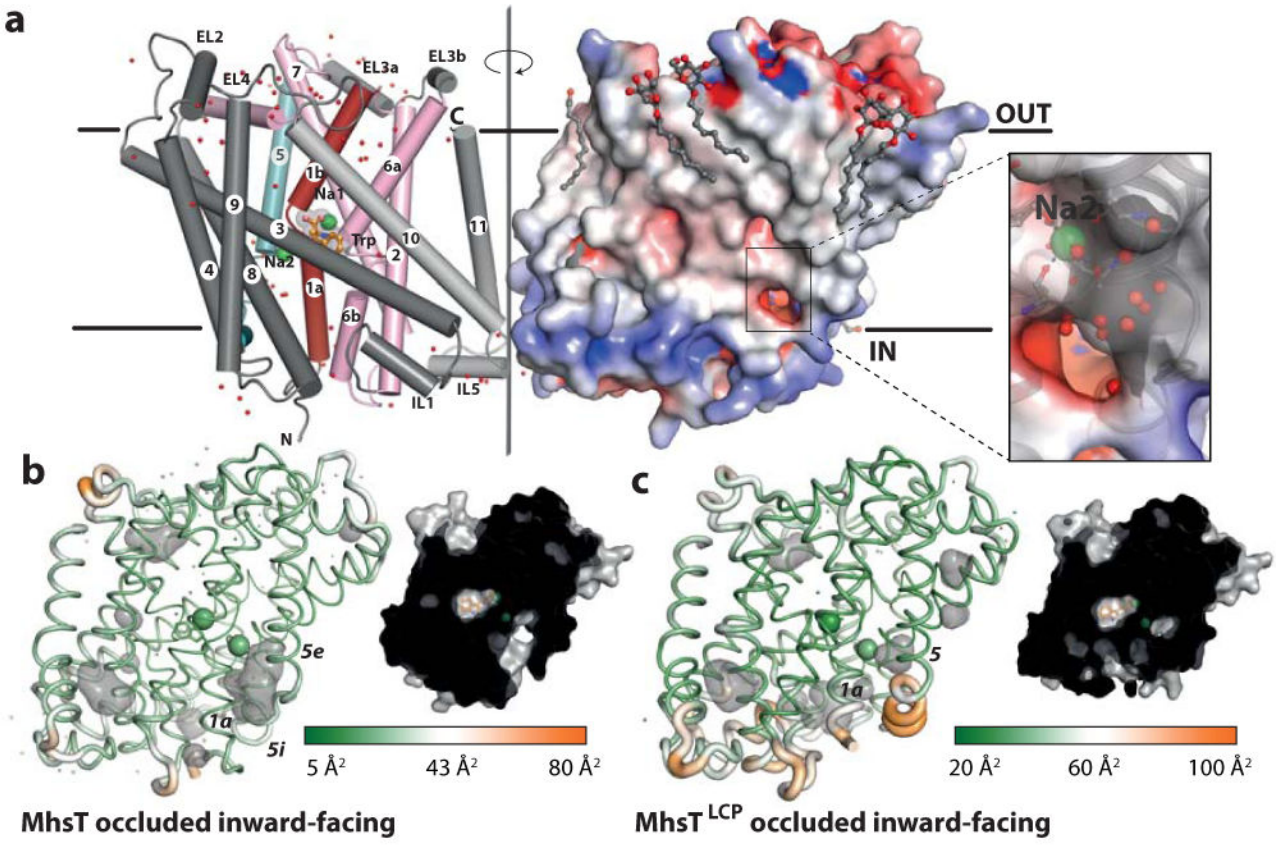

Figure 1. MhsT structure

a, MhsT forms a crystallographic dimer through the intracellular half of helix 11 and intracellular loop 5. MhsT is shown in a schematic representation (scaffold helices in dark grey, bundle helices in red and pink, and TM5 in cyan) with associated water molecules (red dots). The electrostatic surface is shown for the symmetry related MhsT (right side, associated detergent molecules as ball-and-sticks, Na^+ as green spheres, L-Trp as orange sticks) and the close-up shows a cytoplasmic cavity lined by negatively charged residues that reaches the Na2 site. **b-c**, Schematic structures based on HiLiDe (b) and LCP crystallization (c) with cavities (grey, left) and cut-through surface representations (right). Structural flexibility is indicated by the atomic displacement coded cartoon putty thickness and color gradient from green (low disorder) to orange (high disorder), with average values 23.7 $Å^2$ and 46.5 $Å^2$ for MhsT and $MhsT^{LCP}$, respectively

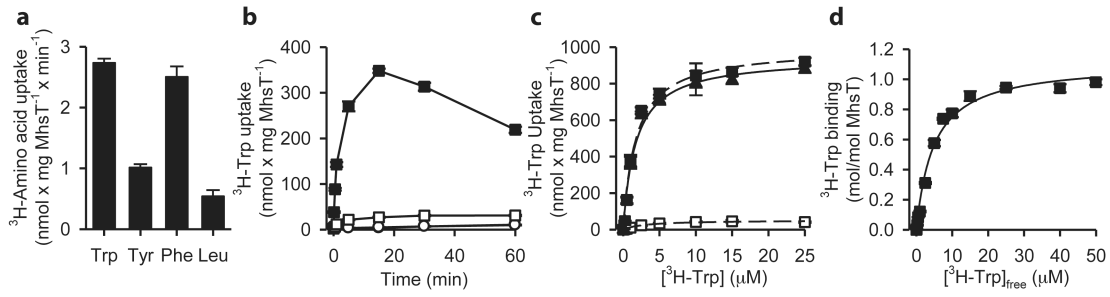

Figure 2. MhsT uptake and binding

The activity of MhsT reconstituted into proteoliposomes was determined by **a**, 1-minute uptake measurements of ^{3}H-Trp, ^{3}H-Tyr, ^{3}H-Phe, and ^{3}H-Leu at 0.1 μM in the presence of NaCl, **b**, a time-course of 1 μM ^{3}H-Trp accumulation. **c**, Kinetics of MhsT-mediated L-tryptophan uptake in proteoliposomes. Initial rates and time course of transport were measured against increasing concentrations of ^{3}H-Trp in the presence of an inwardly-directed Na^+ electrochemical gradient (▪) or by dissipation of the gradient with gramicidin (□, reflecting binding). Net transport (▲) is the difference between total accumulation and binding. The control liposomes (without MhsT, ○) served as control in (b). **d**, Saturation equilibrium binding of ^{3}H-Trp by MhsT was assayed with the SPA of purified, DDM-solubilized MhsT plotted as function of free ^{3}H-Trp. Error bars represent the S.E.M., n=3.

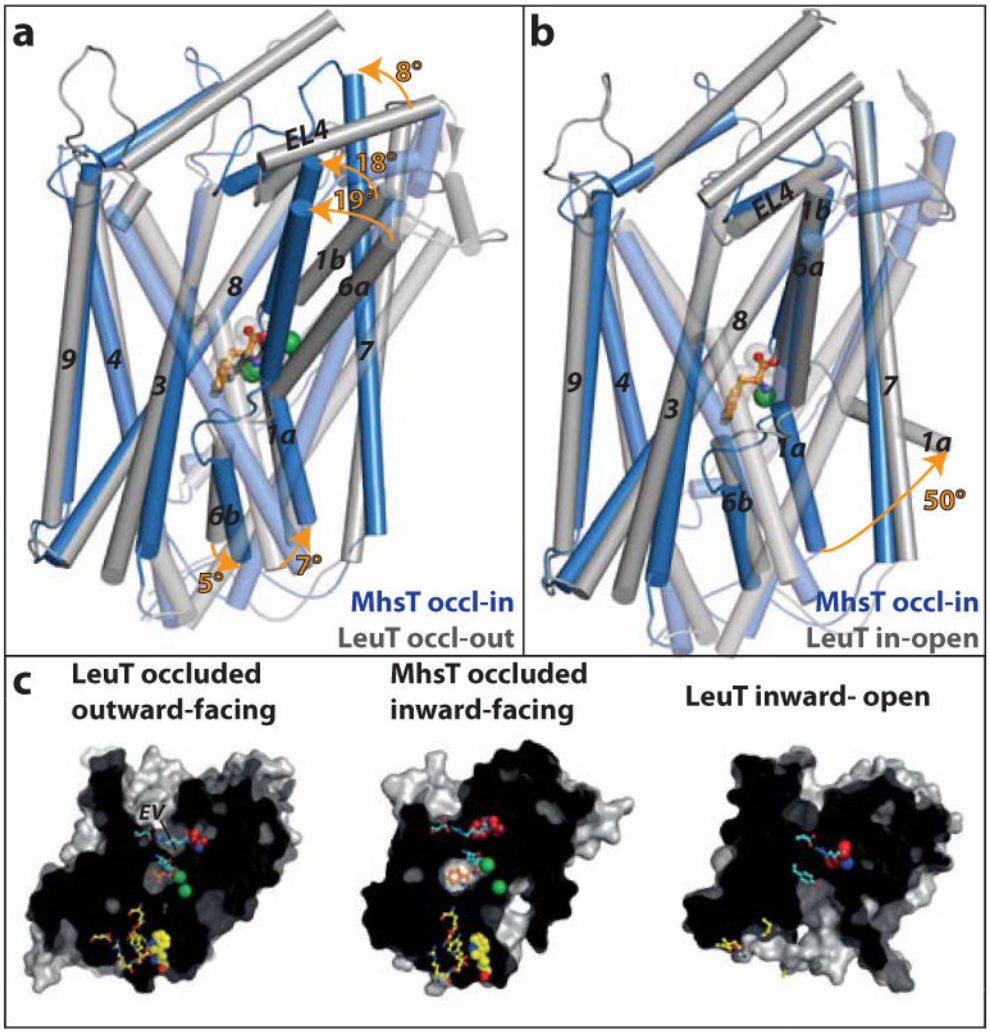

Figure 3. Comparison of MhsT and LeuT in different functional states

a-b MhsT occluded inward-facing (occl-in, blue) is compared to LeuT (a) occluded outward-facing[7] (occl-out, PDB 2A65, grey) and (b) inward-open[10] (in-open, PDB 3TT3, grey) based on superpositioning of the scaffold domains (TMs 3-4, 8-9). Key structural changes are marked with orange arrows. **a**, The switch from outward- to inward-facing occluded states is associated with a movement of the extracellular parts of helices 1b, 6a and 7 and extracellular loop 4 (EL4) towards the scaffold domain that closes the extracellular vestibule. **b**, The switch from occluded inward-facing to inward-open is linked to the release of Na^+ from the Na2 site, which triggers TM1a to swing out and open a wide, intracellular pathway. **c**, Intracellular and extracellular cavities. Residues forming the extracellular gates are colored in cyan ($Arg34^{MhsT}/Arg30^{LeuT}$, $Tyr108^{MhsT}/Tyr108^{LeuT}$, $Phe230^{MhsT}/Phe253^{LeuT}$, $Asp385^{MhsT}/Asp404^{LeuT}$). $Trp33^{MhsT}$ is a key residue of the hydrophobic extracellular vestibule (EV) and is colored red (conserved, except unique $Leu29^{LeuT}$). Intracellular gates ($Arg9^{MhsT}/Arg5^{LeuT}$, $Glu10^{MhsT}/Glu6^{LeuT}$, $Ser244^{MhsT}/Ser267^{LeuT}$, $Tyr245^{MhsT}/Tyr268^{LeuT}$, $Glu330^{MhsT}/Gln361^{LeuT}$, $Asp369^{LeuT}$, $Arg344^{MhsT}/Arg375^{LeuT}$)

are shown in yellow sticks and a hydrophobic plug ($Trp12^{MhsT}$/$Trp8^{LeuT}$) in yellow spheres. The substrate is shown in orange and Na^+ ions in green spheres.

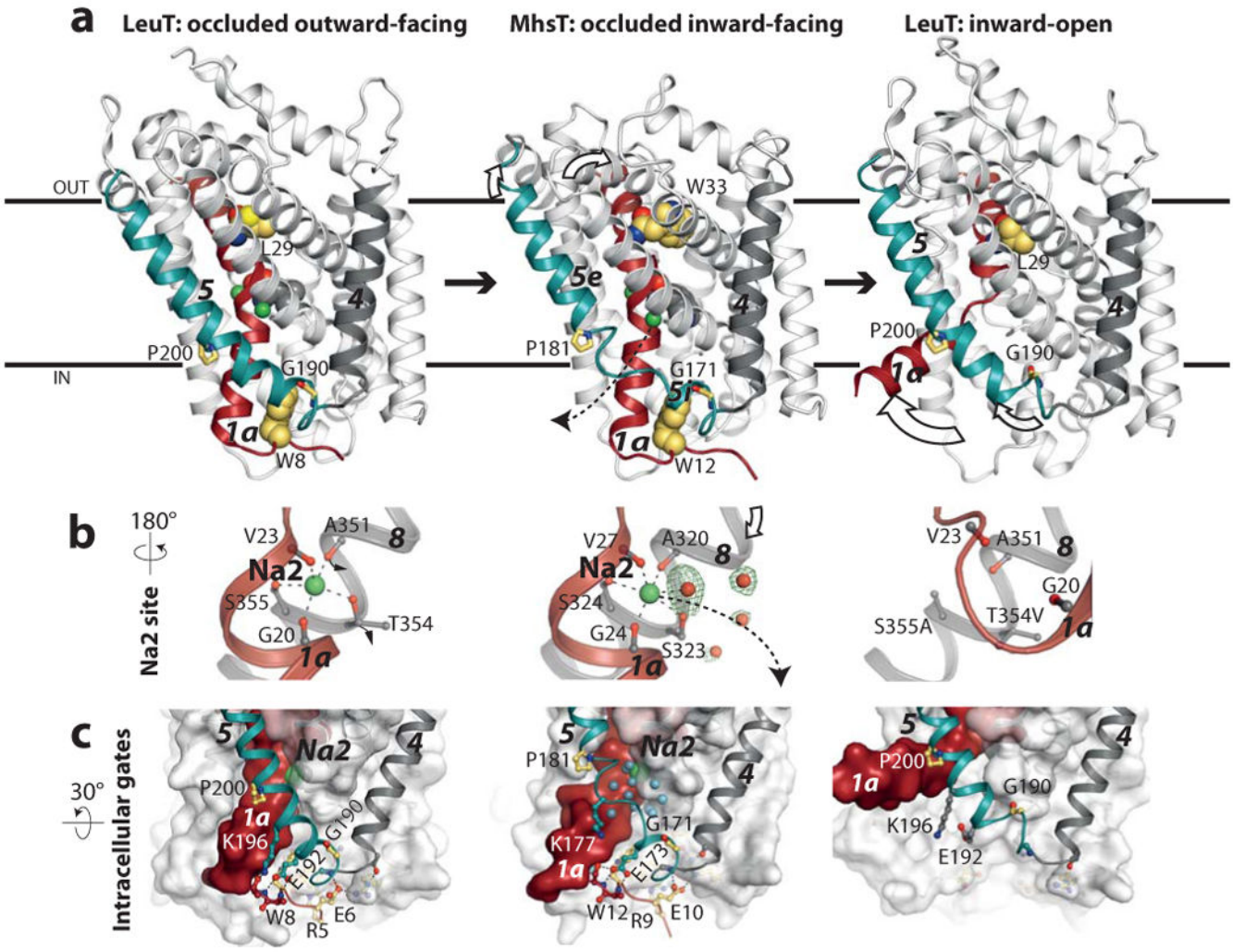

Figure 4. A proposed TM5 "spring mechanism"

Conformational changes depicted by structures of the occluded outward-facing LeuT[7], occluded inward-facing MhsT (this work), and inward-open LeuT[10]. **a**, TM5 (cyan) and TM1 (red) movements (white arrows). **b**, Changes at the Na2 site: trigonal-bipyramidal in the outward-facing LeuT, octahedral in the occluded inward-facing MhsT, and Na^+ released in the inward-open LeuT. A F_o-F_c simulated annealing omit map (3 r.m.s.d. contour in green) shows water molecules in a solvent pathway reaching Na2. **c**, Intracellular gates encompass tight interactions between the N-terminus and TM4-5. Conserved residues in NSS are shown in yellow and waters of the Na2 solvation pathway as cyan spheres. The switch from outward- to inward-facing states occurs by collapse of the extracellular vestibule on the conserved $Trp33^{MhsT}$ that associates with unwinding at the conserved $GlyX_9Pro$ motif at the intracellular side of TM5 next to the Na2 site.

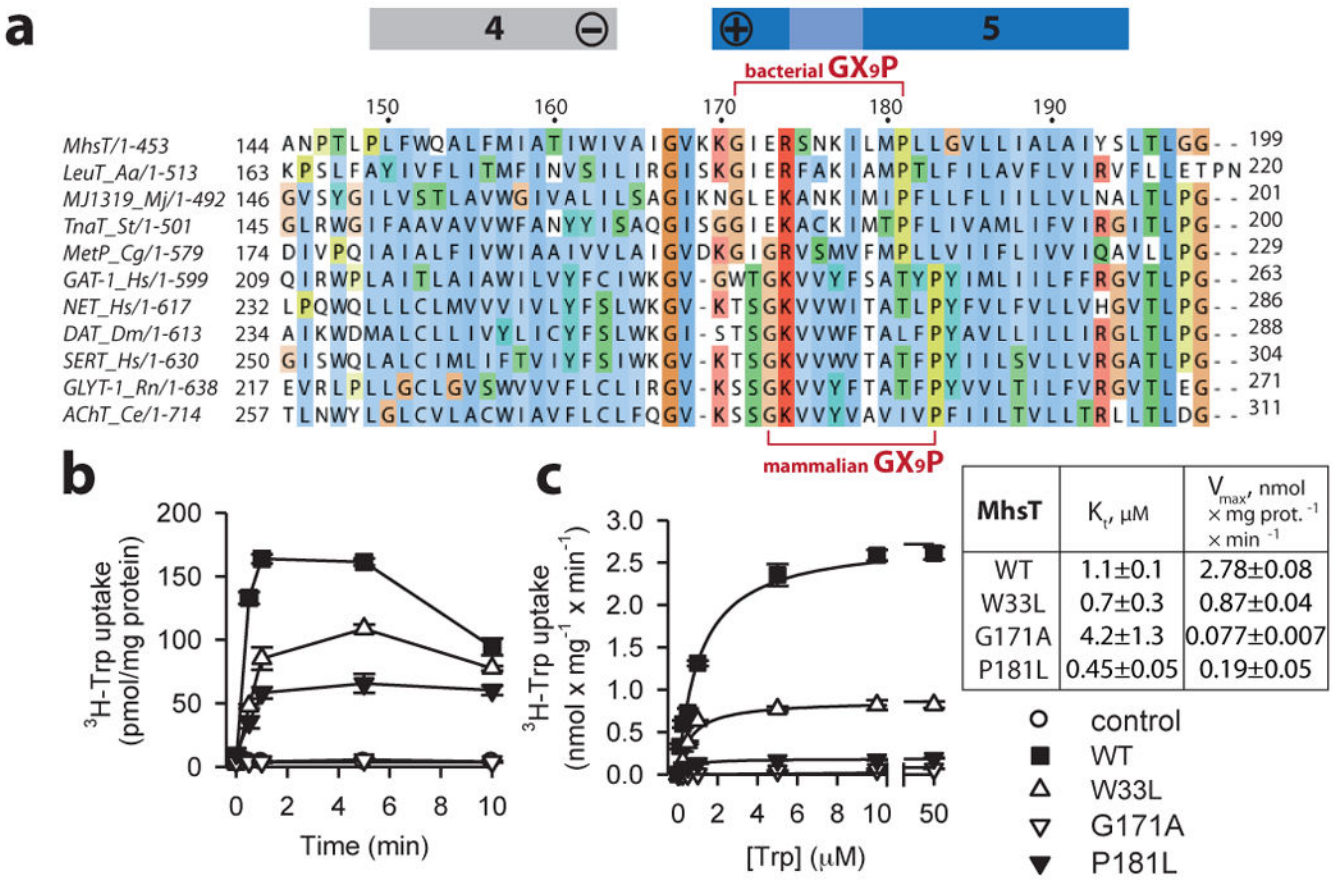

MhsT	K_t, μM	V_{max}, nmol × mg prot.$^{-1}$ × min^{-1}
WT	1.1±0.1	2.78±0.08
W33L	0.7±0.3	0.87±0.04
G171A	4.2±1.3	0.077±0.007
P181L	0.45±0.05	0.19±0.05

Figure 5. Conservation of transmembrane helix 5 GlyX$_9$Pro motif and mutational studies

a, Sequence alignment of the NSS family based on a structural alignment of LeuT, MhsT and dDAT highlighting a conserved GlyX$_9$Pro motif in TM5. **b**, Time course of 0.1 μM ^{3}H-Trp (20 Ci/mmol) accumulation in intact cells of MQ614 expressing WT and mutant MhsT. Uptake was measured in 10 mM Tris/MES pH 8.5 and 50 mM NaCl. **c**, Kinetics of ^{3}H-Trp uptake in intact MQ614 cells expressing MhsT-WT (▪), W33L (△), G171A (▽), and P181L (▾). Symbols are consistent in b and c (control cells lacking MhsT are shown as O in b) and data represent the mean ± SEM of triplicate determinations of representative experiments that were repeated ≥ three times.

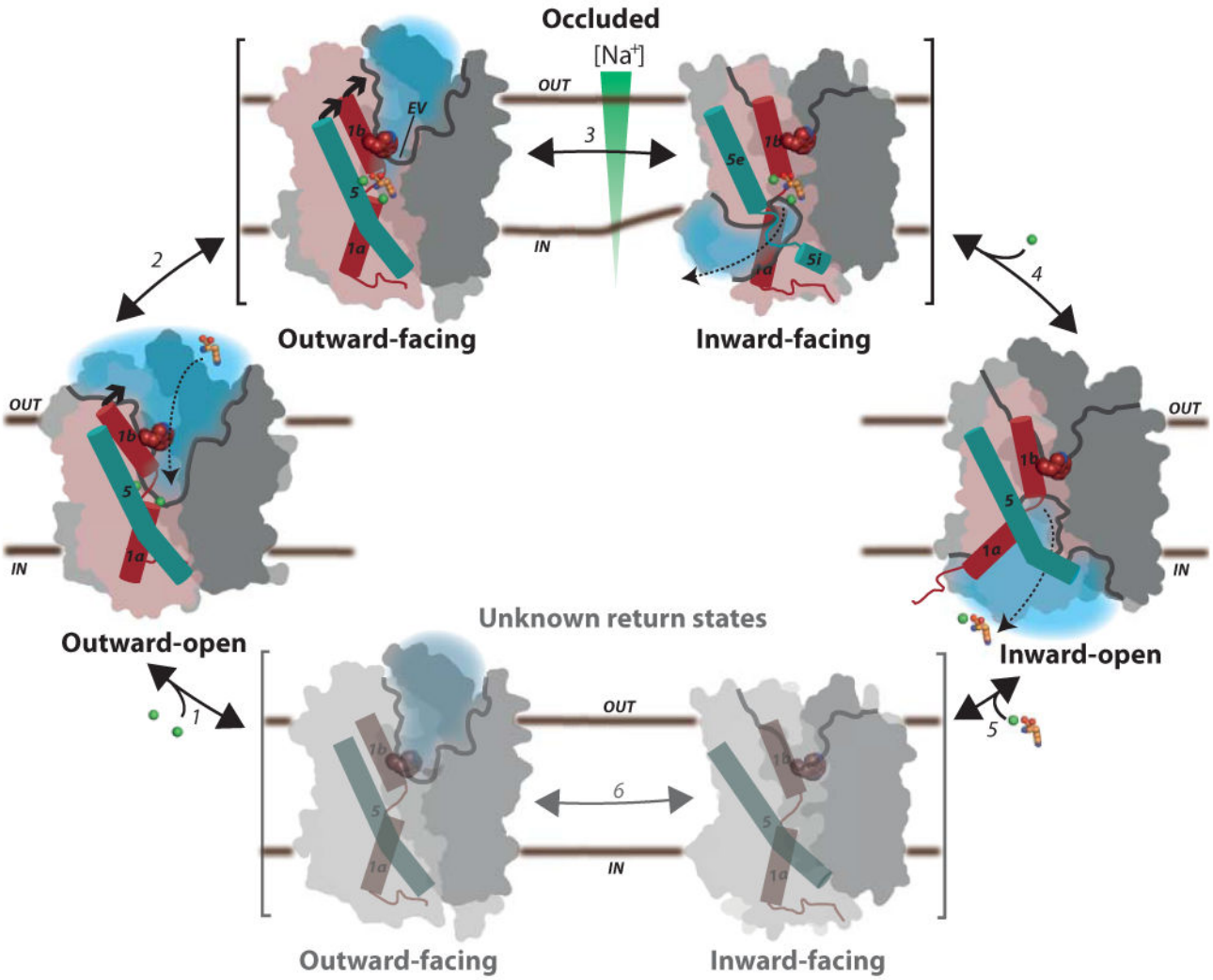

Figure 6. Transport mechanism of the NSS family

Na^+ binding at the Na1 and Na2 sites stabilizes the outward-open state (*1*) and allows the substrate to bind (dashed arrow), triggering substrate site occlusion (*2*). Closure of the hydrophobic extracellular vestibule (EV) on Trp33 facilitates formation of an inward-facing state where TM5 unwinding provides a solvation pathway for the Na2 site (*3*) and an opportunity for Na^+ to escape to the intracellular low-Na^+ environment (*4*). Na^+ release from Na2 allows TM5 to reform and TM1a to swing out to release the substrate with Na^+ from Na1 in the inward-open state. Finally, the transporter switches back to the outward-open state through yet unknown occluded return states (*5*-*6*). Scaffold is shown in dark grey, bundle domain in pink, cavities opening in grey line, and solvated regions in light blue, TM1 as red and TM5 as cyan cylinders, Na^+ ions as green, and amino acid substrate in orange spheres.

Table 1

Data collection and refinement statistics

	MhsT HiLiDe	MhsT LCP
Data collection		
Space group	P2	C2
Cell dimensions		
a, *b*, *c* (Å)	44.3, 49.9, 110.1	44.2, 92.7, 112.5
α, β, γ (°)	90, 96.8, 90	90, 99.5, 90
Resolution (Å)	44.0−2.10 (2.21−2.10)*	39.4−2.60 (2.72−2.60)*
R_{sym} (%)	15.7 (124.3)	15.6 (92.5)
$I/\sigma I$	8.9 (1.15)	5.0 (1.0)
$CC_{1/2}$ (%)#	99.5 (44.0)	97.5 (21.2)
Completeness (%)	98.7 (98.5)	96.8 (97.6)
Redundancy	3.8 (3.8)	2.0 (2.0)
Refinement		
Resolution (Å)	44.0−2.10 (2.21−2.10)	39.4−2.60 (2.72− 2.60)
No. reflections	27,894 (3,907)	13,315 (1,632)
R_{work}/R_{free}	0.191/0.235	0.201/0.255
No. atoms		
Protein	3320	3243
L-tryptophan ligand	15	15
Na^+ ions	2	2
Water	77	22
Detergents/lipids	184	66
B-factors		
Protein	23.7	45.9
L-tryptophan ligand	12.8	30.9
Na^+ ions	14.9	35.2
Water	26.1	41.2
Detergents/lipids	41.7	64.1
R.m.s. deviations	24.4	46.2
Bond lengths (Å)	1.73	0.80
Bond angles (°)	0.012	0.003

*Values in parentheses are for highest-resolution shell.

#Percentage of correlation between intensities from random half-datasets.